Journal of Membrane Science 624 (2021) 119108

Contents lists available at ScienceDirect

Journal of Membrane Science

journal homepage: http://www.elsevier.com/locate/memsci

Fabrication of high-performance pervaporation membrane for sulfuric acid recovery via interfacial polymerization

Huaqing Liu [a], Jianzhong Xia [b,**], Kangjie Cui [a], Junquan Meng [a], Rui Zhang [a], Bing Cao [a], Pei Li [a,*]

[a] College of Materials Science and Engineering, Beijing University of Chemical Technology, Beijing, 100029, China
[b] Institute for Advance Study, Shenzhen University, Shenzhen, 518060, China

ARTICLE INFO

Keywords:
Pervaporation
Acid-resistant membrane
Thin film composite
Interfacial polymerization
Acid wastewater recovery

ABSTRACT

Industrial acid wastewater is one of the top hazardous wastes to environment. Acid-resistant nanofiltration membrane has been applied in acid wastewater reclamation but is limited to the high osmotic pressure for treating concentrated acid solution. On the other hand, pervaporation (PV) technology has been industrialized for dehydration from organic solvents. It has the potential to extract water from concentrated acid solutions. Nevertheless, PV membrane must have excellent acid resistance besides good ion rejection. Here, we prepared a series of thin-film composite PV membranes based on polysulfonamide (PSA)/polyethersulfone (PES). The PSA selective layer was formed by interfacial polymerization (IP) between a polyethyleneimine (PEI)/m-phenylenediamine (MPD) mixed aqueous solution and a hexane solution of m-phenylenedisulfonyl chloride (BDSC). By optimizing the preparation conditions, the PSA/PES membrane exhibited a water flux of 51.1 ± 2.3 kg m^{-2} h^{-1} with a NaCl rejection of 99.60% when desalinating a 35000 ppm NaCl solution at 75 °C. After soaking in 20 wt% H_2SO_4 solution for one month, the desalination performance of the membrane was maintained. Furthermore, the membrane showed a water flux of 47.5 ± 1 kg m^{-2} h^{-1} and a rejection to H_2SO_4 over 99.9% when separated a 10 wt% H_2SO_4 solution at 75 °C for at least 20 h. All these results demonstrate that the thin film composite PV membrane is very suitable for treating concentrated acid wastewater.

1. Introduction

Industrial wastewaters are mainly produced in fermentation process, textile dyeing production, rinsing process, electroplating, etc. [1–3] These wastewaters often contain acids such as HNO_3, H_2SO_4, or HCl [4–6]. Membrane material must have superior acid-tolerance to resist hydrolysis under the attack of protons in acid solution. It is reported that polymers having benzene rings, ether bonds, furan rings, sulfone groups, amides, heterocycles, and sulfonamides, are stable in acid because the strong conjugation effects among their p or π electronic orbits [7–13]. Under this guidance, many acid-resistant polymers have been synthesized and made into membranes.

Liu et al. prepared a thin film composite (TFC) nanofiltration (NF) membrane consisting of a dense polysulfonamide (PSA) layer and a porous polysulfone support [13]. The PSA layer was made by interfacial polymerization (IP) of 1,3,6-naphthalenesulfonate chloride and piperazine (PIP). Because the low polarity of the S═O group and strong conjugation effects, the PSA/PS NF membrane was stable in 20 wt% H_2SO_4 solution. Hamzeh et al. reported that PSA had better acid tolerance thanpolyamide-sulfonamide (PASA) [14].

Other acid-resistant nanofiltration or ultrafiltration membranes, which were prepared using poly(p-phenylene sulfide) (PPS) [14], sulfonated polyethersulfone (SPES) [15], and polyethersulfone ketone (PPESK) [16], either showed limited rejection to ions or not suitable for concentrated acid solutions. On the other hand, pervaporation (PV) technology has potential to treat concentrated acid solution because the driving force is not sensitive to salt or ion contents in feed solutions [17]. Energy efficiency of PV process can be very competitive to reverse osmosis (RO) if renewable or waste heat is applied [18,19]. Moreover, the small foot-print and much better fouling resistance than membrane distillation make PV promising for recycling acid wastewater.

In a previous study, we fabricated a series of PSA/PES TFC

* Corresponding author.
** Corresponding author.
E-mail addresses: xiajianzhong@outlook.com (J. Xia), lipei@mail.buct.edu.cn (P. Li).

https://doi.org/10.1016/j.memsci.2021.119108
Received 21 November 2020; Received in revised form 13 January 2021; Accepted 19 January 2021
Available online 26 January 2021
0376-7388/© 2021 Elsevier B.V. All rights reserved.

membranes [4]. The IP layer was produced by reacting a water solution of triethylenetetramine (TETA) and MPD with a n-hexane solution of m-phenylenedisulfonyl chloride (BDSC). Although the membrane showed stable separation property in 20 wt% H_2SO_4 solution, water flux was only 10.1 kg m^{-2} h^{-1}, which was much lower than the typical water flux (30–40 kg m^{-2} h^{-1}) of RO membranes [20]. We hypnotized that the high crosslinking density and poor hydrophilicity of the MPD/TETA/BDSC PSA polymer caused the low water flux. To solve this problem, we substituted the tri-functional TETA monomer with polyethyleneimine (PEI) in this work. PEI has multiple amine groups and branched polymer structure. Reacting PEI with BDSC shall form branched polymer with more free volume for water transport. Moreover, the remaining unreacted amine groups will increase the hydrophilicity of the PSA layer that facilitate water transport. To avoid over-crosslinking of the IP layer, the bi-functional MPD is added to tune the crosslinking density of the PSA polymer. As a result, the PSA based PV composite membrane with a carefully tailored crosslinking PSA structure is prepared and exhibits 5-fold higher water flux with excellent acid resistance.

2. Experimental

2.1. Materials

Polyethersulfone (PES, Udel P1700) was purchased from Solvay Co., Ltd. Polyvinylpyrrolidone (PVP K-30) was bought from Gobekie Co., Ltd. N-methylpyrrolidone (NMP, purity > 99%), n-hexane (purity > 99%), and concentrated sulfuric acid (H_2SO_4 purity: 98%) were provided by Tianjin Damo Chemical Reagent Factory (China). Polyethylene terephthalate (PET) non-woven was obtained from Shanghai Poly Technology Co., Ltd. Deionized water (DI) was produced using a laboratory equipped water purification system (Smart-Q15). Sodium chloride (NaCl, purity: 99.9%) and Sodium aiginate (SA, purity: CP) was got from Sinopharm Chemical Reagent Co., Ltd. (China). 50 wt% polyethyleneimine (PEI, 70,000) aqueous solution and 1,3-benzenedisulfonyl chloride (BDSC, purity > 98%) were purchased from TCI (China). M-phenylenediamine (MPD, purity: 99.5%) and sodium dodecyl benzene sulfonate (SDBS, purity > 95%) was provided by Shanghai Macklin Biochemical Co., Ltd. Polyethylene (PE) porous membrane was provided from Beijing OriginWater Technology Co., Ltd. (China). All chemicals were used as received.

2.2. Preparation of the PES ultrafiltration membrane

PES ultrafiltration membranes were prepared using the non-solvent induced phase inversion method [14,21,22]. Specifically, a polymer dope consisting of PES, NMP, and PVP in a weight ratio of 20:76:4 was prepared and then cast onto a PET non-woven fabric using a 150 μm scraper at room temperature in a dry environment (the relative humidity was controlled below 20%). A gel-like polymer film with the PET substrate was immersed in DI water to induce phase inversion. After being soaked for 72 h in DI water to completely remove NMP and PVP, the PES membrane was taken out and air-dried in ambient temperature. The PES membrane had an average pore size of 6.08 nm and a porosity of 26.4%. (The pore size measurement was provided in Fig. S1).

2.3. Preparation and characterization of the PSA based composite membranes

2.3.1. Adjusting the parameters for interfacial polymerization (IP)

In a typical IP procedure, a porous substrate was first immersed in an aqueous solution and then transferred into an organic solution to induce polymerization. In this work, the IP process was optimized by adjusting the compositions of water and organic solutions (Table 1) as well as the method to deposit the water phase. As shown in Fig. 1, the aqueous solutions were deposited onto the porous support in three ways, i.e. (a) drop-casting [23], (b) roller-casting, and (c) vacuum filtration.

Table 1
The compositions of aqueous and organic phases for IP polymerization of the composite membranes prepared using the drop-casting method.

Membrane ID	MPD (wt %)	PEI (wt %)	BDSC (wt %)	Casting amount (μL·cm^{-2})
M1	0	3	0.5	9
M2	0.2	3	0.5	9
M3	0.4	3	0.5	9
M4	0.6	3	0.5	9
M5	0.8	3	0.5	9
M6	1.0	3	0.5	9
M7	0.6	0	0.5	9
M8	0.6	1	0.5	9
M9	0.6	2	0.5	9
M10	0.6	4	0.5	9
M11	0.6	5	0.5	9
M12	0.6	7	0.5	9
M13	0.6	3	0.17	9
M14	0.6	3	0.33	9
M15	0.6	3	0.67	9
M16	0.6	3	0.5	7
M17	0.6	3	0.5	11
M18	0.6	3	0.5	13
M19(PE)	0.6	3	0.5	10

In the drop-casting process, a piece of PES or PE membrane (3.5 cm × 3.5 cm) was adhered to a PTFE flat board, and then the aqueous amine (PEI and MPD) solution was uniformly dropped onto the membrane using a micro-pipette. The solution droplets were gently spread over the membrane surface using a casting knife. This method could precisely control the amount of aqueous solution deposited on the surface of the supporting membrane (7–13 μL cm^{-2}). After that, the membrane was set for 30 s. During this period, amine solution submerged into the pores of the substrate. Then, the membrane was immersed into an organic solution for 2 min to complete the interfacial polymerization. At last, the membrane was heated in an oven at 80 °C for 5 min, rinsed with n-hexane and DI water, and air-dried.

In the roller-casting process, the porous substrate was dipped in the amine aqueous solution and taken out. Excess amount of solution was removed by a rubber roller on the substrate surface, which was then soaked in an organic solution and followed the same procedure as preparing the drop-casting composite membrane.

In the vacuum filtration process, a PES membrane was cut into a circle with a diameter of 5 cm. Then, the membrane was mounted into a vacuum filtration device. 10 mL of aqueous solution was poured on top of the membrane, while permeation side of the membrane was vacuumed at 0.2 atm for 5 min. Note that, due to the high molecular weight of PEI, pores of the substrate was immediately blocked so that most of the aqueous solution was retained on the membrane surface. After poured out the aqueous solution, the membrane was taken out from the filtration device and immersed into an organic solution for 2 min for interfacial polymerization. Then, the membrane underwent the same treating procedures as the roller-casting and drop-casting methods.

2.4. Characterizations

Morphologies of the PV composite membranes on PE and PES supports, denoted as PSA/PE and PSA/PES, respectively, were observed using a JEOL jsm-7401f (Japan) Scanning Electronic Microscope (SEM). Samples were fractured in liquid nitrogen to obtain a smooth cross-section and sputter-coated with gold before test. Chemical structures of the PSA layers were determined by monitoring their Fourier Transform Infrared (FTIR) spectra using an infrared spectrophotometer (Nicolet IS5, ThermoScientific, USA). The FTIR spectra were recorded in the range of 4000–500 cm^{-1} with a resolution of 64 and a penetration depth of 0.92–0.11 μm (a detailed explanation could be found in supporting information). A XPS (ESCALAB 250, ThermoFisher Scientific,

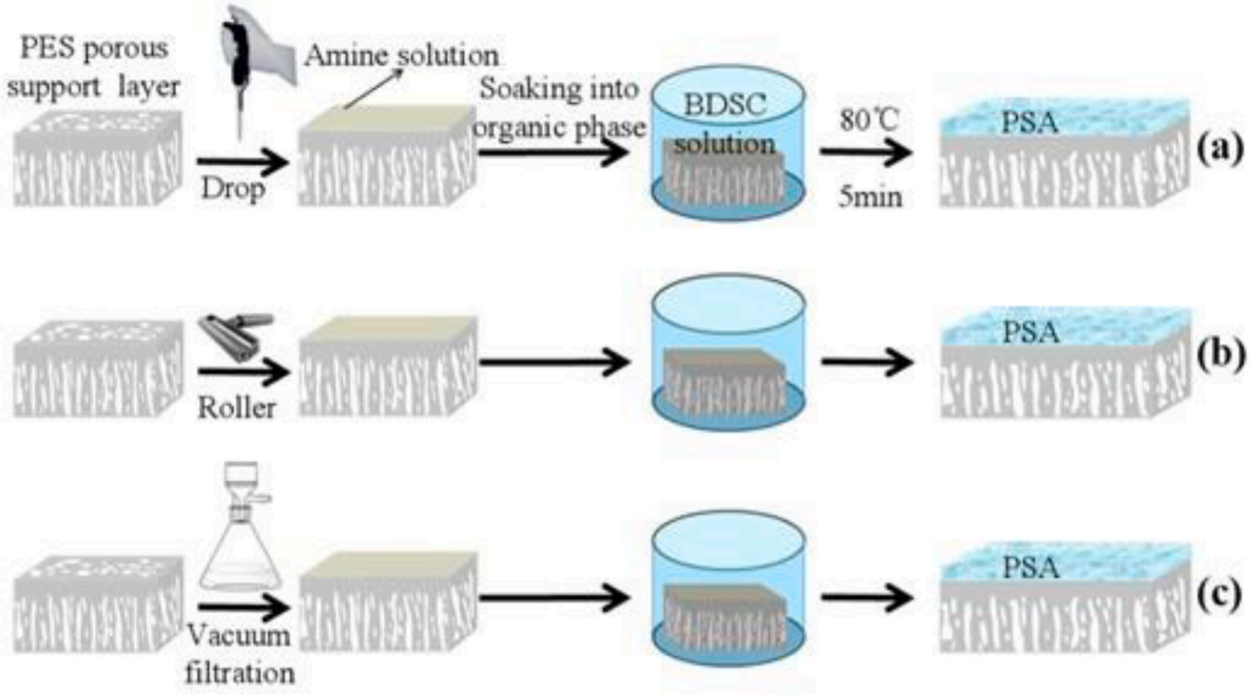

Fig. 1. The schematic diagrams of three IP processes: (a) drop-casting, (b) roller-casting and (c) vacuum filtration.

USA) equipment was used to analyze the electron energy at a penetration depth of 10 nm. All membrane samples were vacuum dried at 100 °C overnight before characterization. Hydrophilicity of the PEI containing PSA was evaluated using a contact angle goniometer (DSA 100, KRUSS, Germany). Triplicated tests were performed for each sample and the average values were adopted. The membrane surface (5 μm × 5 μm) roughness was measured by an Atomic Force Microscopy (AFM) (S-7800, HITACHI, Japan).

2.4.1. Pervaporation tests

Separation properties were measured using a bespoke PV equipment as shown in Fig. 2a. The efficient transport area of the PV membranes was 2.83 cm^2. The feed solutions, 35000 ppm NaCl, 10 wt% H_2SO_4, or 35000 ppm NaCl with 0.1 wt% organics of sodium alginate (SA) or sodium dodecyl benzene sulfonate (SDBS), were circulated on the membrane feed side at 75 °C. To mitigate the concentration and temperature polarization effects, the flow rate of the feed solution was controlled at 0.1 m s^{-1}, corresponding to a Reynolds' number of 6122 that indicating a turbulent flow state (a detailed calculation procedure was provided in supporting information) [24]. Membrane permeate side was in a vacuum of 100 Pa to draw over water vapor that was condensed in a nitrogen cold trap. Membrane flux (J, kg·m^{-2}·h^{-1}) was calculated by Eq. (1).

$$J = \frac{M}{A_0 \times t} \tag{1}$$

where M was mass (kg) of the water vapor collected in the cold trap; A_0 was effective membrane area (m^2); and t was the testing time (h). Salt rejection (R) was calculated using Eq. (2).

$$R = \frac{(C_f - C_p)}{C_f} \times 100\% \tag{2}$$

where C_f and C_p represented the salt concentrations of the feed and permeate solutions. Salt concentration in the feed was directly measured using a conductivity meter (Oakton® Con 110). Salt concentration in the permeate side was measured in an indirect way since it was non-volatile. The collected water in the cold trap was used to wash the membrane permeate side to dissolve any permeate salt. The conductivity was measured to get C_p. Each experimental condition was repeated for at least three times and the standard deviation was calculated.

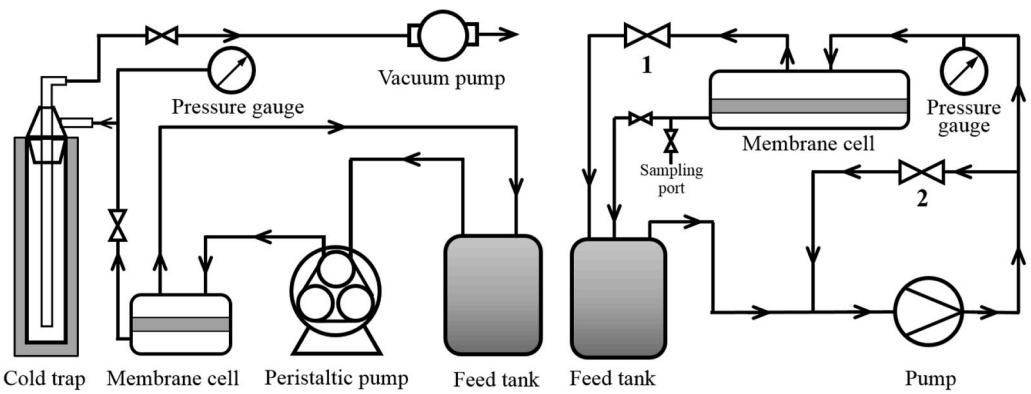

Fig. 2. (a) Schematic diagram of the pervaporation test device; (b) pure water flux measurement device.

2.4.2. Determination of the pure water flux to the PE and PES membranes

The pure water fluxes of the PE and PES membranes were measured using a cross-flow ultrafiltration testing device. A schematic diagram is shown in Fig. 2b. At the beginning of the test, the membrane was pressurized at 2 bar for 30 min. Then the feed pressure was reduced to 1 bar and the pure water flux was obtained using Eq. (1) where M was mass (kg) of the water collected at a certain time, A_0 was effective membrane area (m^2), and t was the testing time (h).

2.5. Calculation of the activation energy

The apparent activation energy of water transport in PV desalination membranes was calculated using Eq. (3):

$$J = J_0 \exp(-\frac{\Delta E}{RT}) \quad (3)$$

where J referred to water flux; J_0 was the pre-exponential factor; $\triangle$E was the activation energy ($kJ \cdot mol^{-1}$); R was gas constant (8.314 J mol^{-1} K^{-1}); and T was temperature (K).

2.6. Acid tolerance tests

Acid tolerance of the PSA based composite membranes was evaluated using both static and dynamic tests. In the static tests, the PSA/PES composite membranes were soaked in a 20 wt% H_2SO_4 solution for one month. During that time, the membrane was rinsed with DI water and tested for desalination properties every five days. The water flux and salt reject before and after soaked in H_2SO_4 were compared to assess the membranes' stability. The dynamic acid tolerance tests were carried out by using a relatively dilute 10 wt% H_2SO_4 solution as the feed solution (for safety concern) for PV experiment at 75 °C. Membrane flux and conductivity of the permeate water were continuously measured for 20 h to assess the membrane's stability in acid solution.

2.7. Mechanical properties tests

The mechanical properties of PSA/PES composite membranes were measured by a tensile test, which were performed using DMA (Q800, TA Instruments, USA). The specimen was made into a long strip of 7 mm wide and 20 mm long. All specimens were mounted between two clamps where the upper clamp was fixed and the lower clamp moved at a constant growth rate of 0.4 N/min. The program automatically recorded the tension and deformation in real time and generated the stress-strain curve.

2.8. Anti-fouling performance tests

3.5 wt% NaCl solution was added with 0.1 wt% organic pollutants (SA, a major organic pollutant in water treatment or SDBS, an anionic surfactant). Flux and rejection to the solution using the PSA composite membrane were measured before and after the acid treatment. The percentage flux change over time was calculated using Eq. (4):

$$\alpha(\%) = \frac{F_t}{F_0} \times 100 \quad (4)$$

whereF_t was the water flux at t time; F_0 was the pure water flux.

3. Results and discussion

3.1. Confirmation of the chemical structure of PSA

Fig. 3a shows the chemical structure of the PSA derived from MPD,

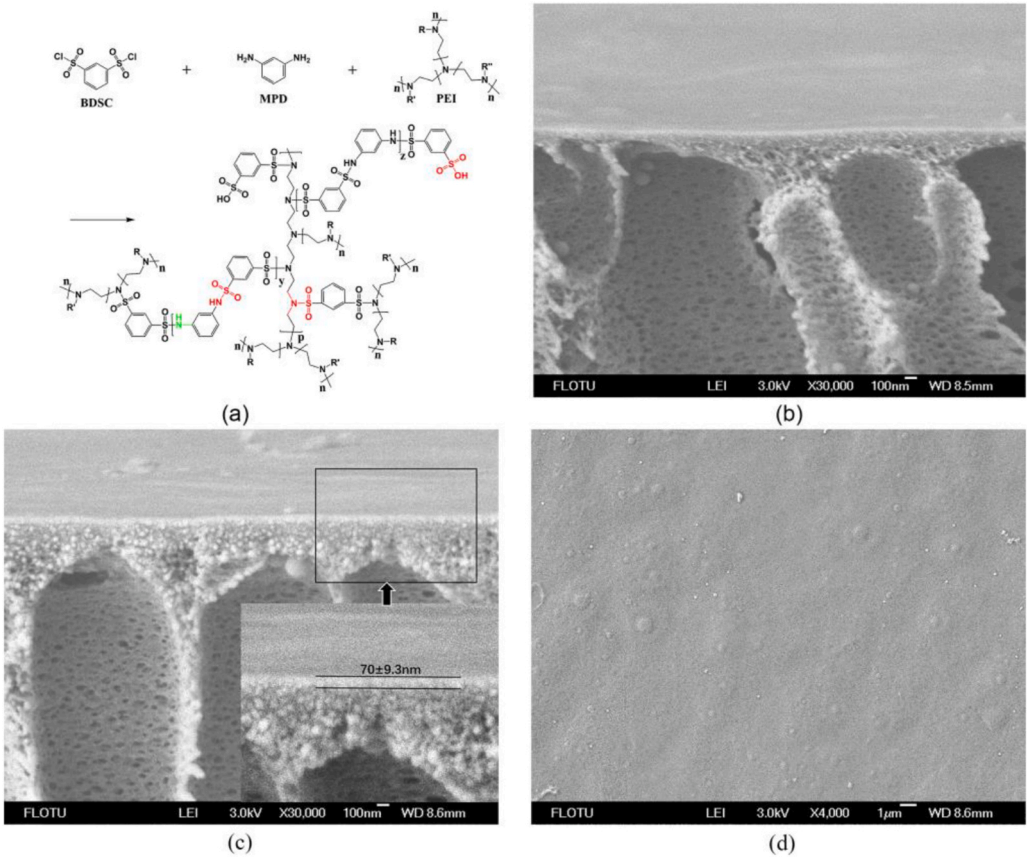

Fig. 3. (a) the synthesis route of polysulfonamide from MPD, PEI, and BDSC (R and R′ denote alkyl or H groups); (b, c) the SEM cross-section images of the PES and M4 composite membranes; (d) the surface SEM image of the M4 composite membrane.

PEI, and BDSC. The chemical reactions of MPD/BDSC and PEI/BDSC will form two types of sulfonamides, i.e. Aryl-N-sulfonamide and tertiary sulfonamide. As shown in Fig. 4, compared with the FTIR spectra of MPD, PEI, and BDSC, there are four new peaks at 1323 cm^{-1}, 1150 cm^{-1}, 872 cm^{-1} and 719 cm^{-1} can be observed. They represent the asymmetric and symmetric tensile vibrations of the sulfonamide group [4,11,13,25,26]. In addition, the peak at 872 cm^{-1} is attributed to the tertiary sulfonamide groups [1], and the peak at 1297 cm^{-1} denotes the Aryl-N group [26]. All these results prove the successful formation of PSA from MPD, PEI, and BDSC. The SEM images of the cross-section and surface morphologies of M4 are shown in Fig. 3b, c. It can be seen that the thickness of the PSA layer is about 70 ± 9.3 nm and the membrane surface is defect-free. Moreover, there is no clear boundary between the PSA top layer and the PES support. This is due to that some of the PSA polymer forms inside the pores of the PES support during the IP process. This produces a wedge structure in the support layer and improve the adhesion between the PSA and the PES layers. Therefore, delamination does not occur throughout the experimental period.

3.2. Optimizing the structures of the PSA/PES composite PV membranes

Desalination properties including salt rejection and water flux of the TFC PV membranes are affected by the transport resistance of the supported layer, crosslinking structure and thickness of the PSA layer. Therefore, we adjust the composition of the aqueous phase and organic solution, the amount of aqueous solution being deposited on the support layer, and the way to deposit the aqueous solution to optimize the crosslinking structure and thickness of the thin film composites. We have adopted two chemical stable substrates, PES and PE, to investigate the effects of transport resistance of the supported layer to water flux of the composite membranes.

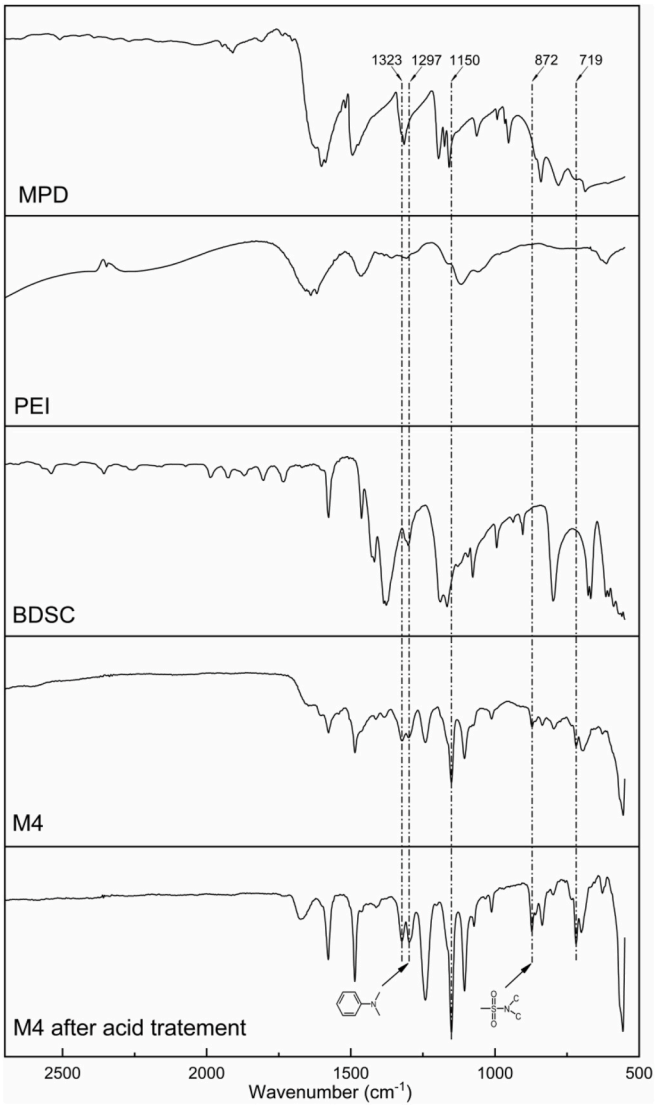

Fig. 4. The FTIR spectra of the MPD, PEI, BDSC and surface of the M4 composite membranes before and after acid treatment.

3.2.1. Effect of the MPD concentration on desalination performance

As shown in Fig. 5a, the M1 composite membrane, which is prepared by IP using an aqueous solution of 3 wt% PEI and a 0.5 wt% BDSC hexane solution, has the lowest membrane flux of 15.5 kg m^{-2} h^{-1} and a salt rejection of 99.7%. As MPD is added to the aqueous solution, membrane flux monotonically increases but the salt rejection decreases rapidly when the MPD concentration increases to 0.8 and 1.0 wt%, indicating defects form in the PSA layers. PEI has an average molecular weight of 70,000. One PEI molecule has roughly 1428 secondary amine groups that can react with BDSC and form hyper-crosslinked network. On the other hand, react MPD with BDSC shall form linear PSA polymer, since both monomers are bifunctional. Due to the smaller molecular size of MPD than PEI, MPD diffuses faster to the organic solution than PEI does [27]. As a result, the BDSC molecules are more likely to react with MPD than PEI. Since the PSA polymer can be crosslinked by PEI only, we expect that increasing the content of MPD in the aqueous solution will reduce the crosslinking density of the PSA polymer and increase the membrane flux. However, at the high MPD concentrations of 0.8 and 1.0 wt%, the low crosslinking density of the PSA layer results in the low salt rejections.

The crosslinking densities of the PSA polymers are determined by XPS analysis, as shown in Fig. 5b. We hypothesize that the higher the crosslinking degree the more the sulfonyl chlorides turn into sulfonamides. On the other hand, the unreacted sulfonyl chlorides will be hydrolyzed and form SO_3H groups. Therefore, by analyzing the XPS spectra of the PSA polymer, it is able to determine the peak area of S in the sulfonamide group (m) located at 168.9 eV, and the peak area of S in SO_3H (n) located at 167.7 eV [28]. Then, the percentage crosslinking degree can be calculated using Eq. (5):

$$crosslinking\ degree\ (\%) = \frac{m}{m+n} \times 100 \quad (5)$$

As listed in Table 2, the crosslinking degrees of the PSA polymers decrease with the increment in the MPD content. This result agrees well with the salt rejection data.

3.2.2. Effect of the PEI concentration on desalination performance

A higher PEI concentration in the PSA polymer leads to a higher crosslinking density and salt rejection. However, the membrane flux does not decrease with the crosslinking density. As shown in Fig. 6a, as the PEI concentration in the aqueous phase increases from 0 to 7 wt% while the MPD concentration is fixed at 0.6 wt%, the membrane flux monotonically increases from 37.2 to 60.1 kg m^{-2} h^{-1}, while the salt rejection first increases and then decreases. The flux increment can be explained by the enhanced hydrophilicity of the PSA polymer. Fig. 6b shows that the water contact angle of the PSA layer surface decreases from 97.9° to 36.8° as the PEI concentration increases from 0 to 7 wt%. Since one PEI molecule has roughly 1428 secondary amine groups, many of them are not reacted with BDSC. These residual amines increase the hydrophilicity of the PSA polymer and water flux [29,30]. According to the Wenzel Equation, surface roughness plays an important role on contact angle [31]. Specifically, an intrinsically hydrophilic material will be more hydrophilic as its surface roughness increases. The AFM images of the PSA/PSE composite membranes (Fig. 6c) demonstrate that adding PEI increases surface roughness of the membranes. Since PEI has secondary amines and MPD has primary amines, the difference in their

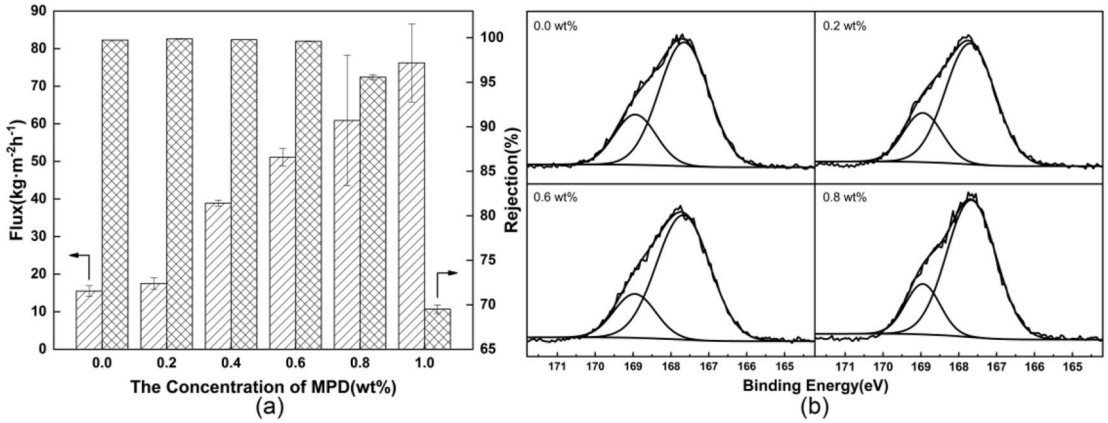

Fig. 5. (a) Water fluxes and salt rejections of the PV composite membranes prepared using different MPD concentrations (feed temperature: 75 °C, permeate side pressure: 100 Pa). (b) the XPS spectra of S2p of four PSA polymers.

Table 2
The MPD concentrations, characteristic peak areas of the XPS spectra, and the crosslinking degree% of the PSA polymers.

MPD (wt%)	m	n	Crosslinking degree (%)
0	2197.70	6518.55	25.21
0.2	2006.09	6307.24	24.13
0.6	1921.14	6988.67	21.56
0.8	1826.01	7104.28	20.45

activities to react with BDSC will lead to the different grown speed of the PSA polymer on surface of the substrate and the increment in roughness [31]. In summary, both the incorporation of hydrophilic amine groups and the increment in surface roughness lead to the formation of more hydrophilic PSA layers of the composite membranes and the high membrane flux. Note that, as the PEI concentration exceeds 3 wt%, the salt rejection starts to decreases. This may be due to that the IP reaction rate is too fast at the high amine concentrations. Since IP is a self-inhibition reaction, the initially form PSA layer will prevent the diffusion of more amines from the aqueous phase to the organic phase. At a high PEI concentration, the nascent PSA polymer will form very

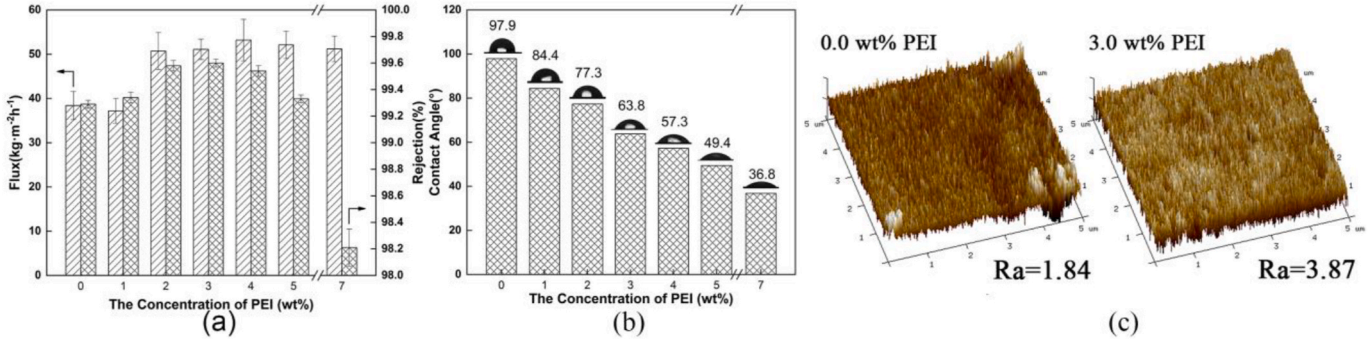

Fig. 6. Prepared PV composite membrane by using different PEI concentrations, (a)Water fluxes, salt rejections (feed temperatures: 75 °C, permeate side pressure: 100 Pa), (b) contact angle, (c) the AFM images of the surface roughness of the 0 and 3 wt% PEI based membranes surfaces.

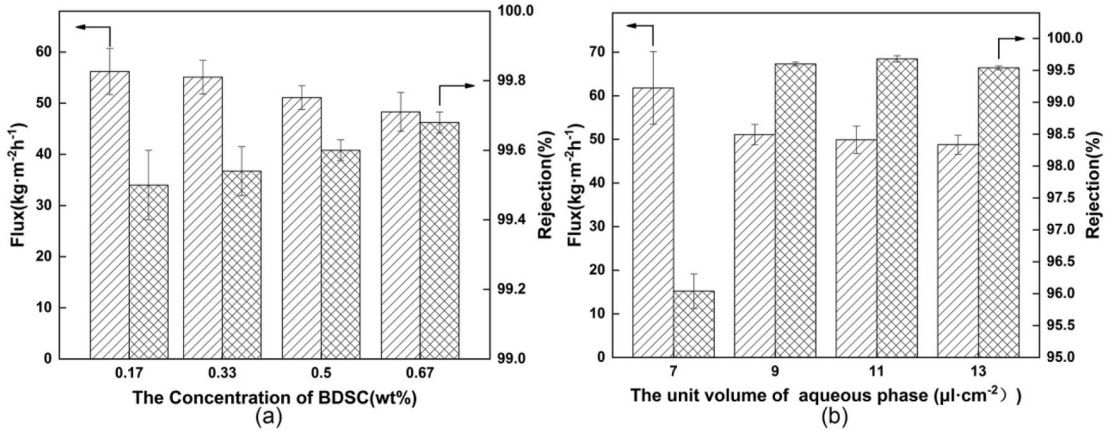

Fig. 7. (a) Effect of BDSC concentration and (b) coating amount of water phase on desalination performance of the thin film composite membranes. (the feed temperatures was 75 °C, permeate side was in a vacuum of 100 Pa).

quickly and have a loosely packed hypo-crosslink structure. This process is analogous to the fabrication of porous hypo-crosslinked polymers [32]. After analyzing the impact of PEI concentration to the desalination property, the desired PEI concentration shall be at the range of 2–5 wt%.

3.2.3. Effect of the BDSC concentration on desalination performance

Fig. 7a shows the membrane fluxes and salt rejections of the composite membranes prepared at different BDSC concentrations. As the BDSC concentration increases from 0.17 to 0.67 wt%, the membrane fluxes gradually decrease from 56.2 to 48.3 kg m^{-2} h^{-1} and the salt rejections increase from 99.5% to 99.7%. This phenomenon can be explained by the increment in the crosslinking density of the PSA as the BDSC concentration increases.

3.2.4. Effect of the casting amount of water phase on separation performance

Using the drop-casting method, the casting amount of aqueous solution could be controlled precisely. Fig. 7b shows the salt rejection is low as the casting amount is 7 μL cm^{-2}. This is due to that there are insufficient amine monomers to react with BDSC and form a defect-free PSA layer. When the casting amount exceed 9 μL cm^{-2}, the salt rejection is higher than 99.5% and the membrane fluxes are similar (51 ± 2 kg m^{-2} h^{-1}). Therefore, the amount of casting solution shall exceed 9 μL cm^{-2} to obtain a defect-free PSA layer.

3.2.5. Comparing the impact of deposition methods of the aqueous solution on desalination performance

Based on the previous results, the parameters for interfacial polymerization are determined where a water solution containing 0.6 wt% MPD, 3 wt% PEI, and a n-hexane solution with 0.5 wt% BDSC are selected. This recipe is adopted to prepare the TFC membranes where the aqueous phases are deposit on the PES substrate using the traditional roller-casting method and vacuum assisted filtration method. Fig. 8a shows that the membrane fluxes prepared using the above two methods are 34.0 and 38.3 kg m^{-2} h^{-1}, respectively, both of which are significantly lower than the M4 membrane prepared using the drop-casting method. In the roller-casting or vacuum filtration processes, the aqueous solution penetrates deeply into the porous substrates under pressure. As a result, the upper part of the porous support is filled by the PSA polymer during IP and the mass transfer resistance of the composite membranes increase. Therefore, the drop-casting method is adopted to prepare the TFC PV membranes. We believe that the aqueous solution can be automatically cast onto a flat-sheet porous support for large-sale membrane preparation.

3.2.6. Effect of the support layers' resistances on desalination performance

Unlike reverse osmosis membranes, substrate resistance plays a very important role in water flux of PV desalination membranes [33–35]. In this study, a commercial polyethylene membrane (average pore size of 0.078 μm and a porosity of 20%) is selected also in concern of its intrinsically good chemical resistance. The PE membrane is treated with corona to increase its hydrophilicity. And a decrement in the water contact angle from 112.6° to 88.2° is observed. However, the pure water flux of the PE membrane is 124.73 kg m^{-2}·h^{-1}·bar^{-1}, lower than that of the lab-made PES membrane of 215.81 kg m^{-2}·h^{-1}·bar^{-1}. Fig. 8b shows that the PSA/PE composite membrane has a low water flux of 32.8 kg m^{-2} h^{-1} and a rejection to NaCl of 99.82%. The result again demonstrates the importance of reducing substrate resistance for preparing PV desalination membranes with high water flux.

3.3. 3.3 Comparison of the activity energies and membrane fluxes of the PSA/PES (M4) membrane to the representative PV desalination membranes

Fig. 9 shows the temperature dependence of water flux to the M4 membrane and other representative PV desalination membranes. In all cases, the water flux increases with temperature. This phenomenon is caused by two reasons: first, the increments in feed temperature increase

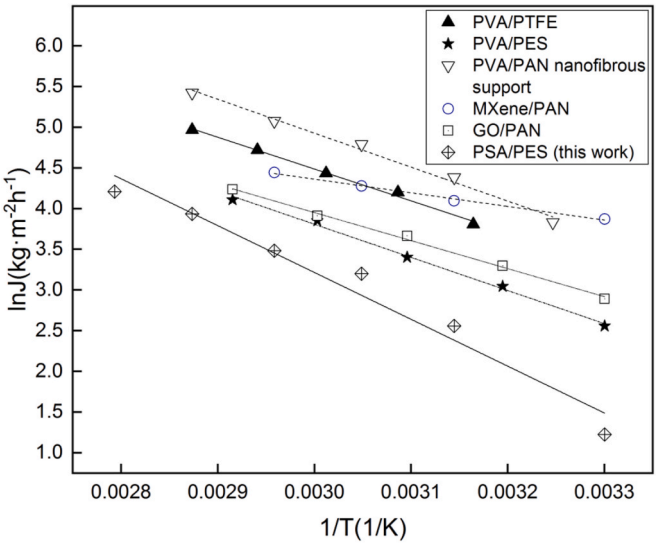

Fig. 9. The Arrhenius plots of the water flux and temperature of PV desalination membranes using a 35000 ppm NaCl solution as feed. Data of PVA/PES, GO/PAN, MXene/PAN, PVA/PTFE, and PVA/PAN nanofibrous support composite membranes are got from Refs. [33–37].

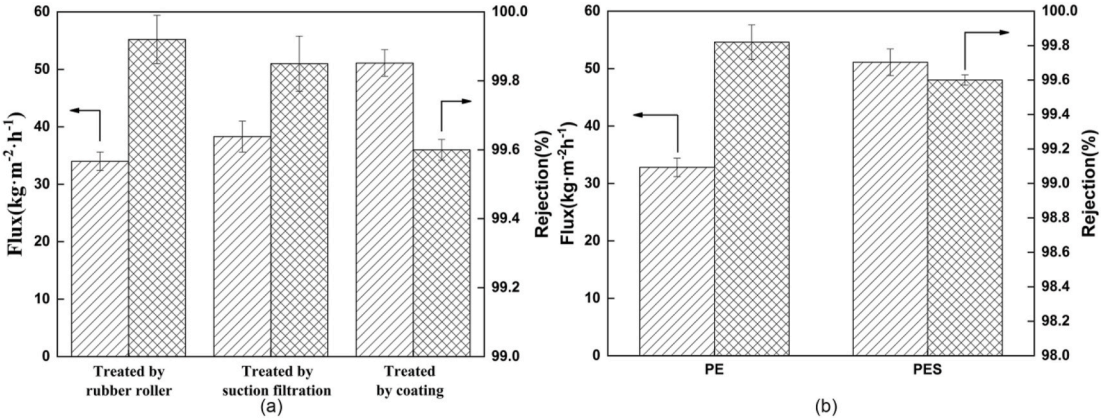

Fig. 8. Effect of water solution (a) deposition methods and (b) porous substrates to desalination properties of the thin film composite membranes. (feed temperature: 75 °C, permeate side pressure: 100 Pa).

water vapor pressure at the membrane feed side so that the driving force for water transport increases; second, the diffusivity of water molecule increases with temperature resulted from the increase in polymer chain flexibility. Although water flux can be enhanced by simply increasing feed temperature, the flux growing rates of membranes vary significantly. The sensitivity of membrane flux to temperature can be analyzed by calculating the apparent activation energy using Eq. (3). According to Table 3, there are 5-fold differences in water fluxes among the six PV desalination membranes (51.1–211 kg m^{-2} h^{-1}). Nevertheless, the activation energies among similar membrane materials are very close. For aliphatic polymer (PVA) based membranes, their activation energies are 32.5–33.8 kJ mol^{-1}, while the 2D inorganic materials, graphene oxide and MXene, exhibit the lowest activation energies of 20.9 and 13.9 kJ mol^{-1}, respectively. The low activation energy of 2D materials indicates that their smooth and hydrophobic surface favors diffusion of the water molecule. On the other hand, the highest activation energy of the PSA/PES membrane stems from the aromatic hyper-crosslinked structure of PSA that restricts the diffusion. The dense layer thickness of PSA/PES membrane is 70 nm, a typical thickness of interfacial polymerization membranes [38,39]. Further decrease in dense layer thickness will be difficult. However, water flux can be improved by reducing the activation energy of the dense layer material. According to Table 3, this can be realized by designing an interfacial polymerization layer using hydrophilic and flexible aliphatic structure (like PVA) or incorporating 2D materials. This methodology will be attempted in our future study.

3.4. Acid resistance of the composite membrane

Acid resistance of the M4 membrane is evaluated in both static and dynamic acid resistance tests. Fig. 10a shows that both water flux and salt rejection maintain after the membrane is soaked in 20 wt% H_2SO_4 for one month. Moreover, a stable water flux of 44.5 ± 1 kg m^{-2} h^{-1} with a H_2SO_4 rejection over 99.9% was obtained during a 20 h experiment at a temperature of 75 °C (Fig. 10b). Moreover, when a piece of PSA/PE composite membrane is immersed in a 20 wt% H_2SO_4 solution for 240 days, the desalination performance is found to be unchanged (Fig. 10c). Therefore, both the PSA/PES and PSA/PE composite membranes have sufficiently high acid resistance and can be used for acid wastewater treatments.

The acid tolerance of the PSA polymer is determined by comparing its FTIR spectra before and after being soaked in a 20 wt% H_2SO_4 solution for one month. It is found that no observable changes in the FTIR spectra after the acid treatment (Fig. 4.), especially for the sulfonamide groups at 1323 cm^{-1}, 1150 cm^{-1}, 872 cm^{-1} and 719 cm^{-1}, respectively. This observation demonstrates that the sulfonamide crosslinking sites have excellent acid resistance. As shown in Fig. 10d, the fracture strain of the M4 membrane decreases from 11.2% to 7.0% and the tensile strength decreases from 3.9 to 3.7 MPa after it is soaked in 20 wt% H_2SO_4 for one month. The mild decrement in mechanical property is mainly attributed to the good chemical stability of PES substrate. To evaluate the mechanical strength of the composite membrane, we used a dead-end test device to pressurize the membrane. The membrane was not fractured at a trans-membrane pressure of 4 bar. Note that, the trans-membrane pressure of PV process is less than 1 bar, the composite membrane shall be stable.

Table 3
Desalination properties and activation energies of representative PV desalination membranes using a 35000 ppm NaCl solution as feed.

Membrane	Temperature (°C)	Water flux ($kg \cdot m^{-2} \cdot h^{-1}$)	Dense layer thickness (nm)	Activation Energy ($kJ \cdot mol^{-1}$)
PSA/PES (M4)	75	51.1	70	47.8
PVA/ nanofibrous support [33]	75	211	730	33.5
PVA/PES [34]	70	60.8	1140	33.8
PVA/PTFE [35]	75	143	2600	32.5
GO/PAN [36]	70	59	80	20.9
MXene/PAN [37]	65	85	60	13.9

Salt rejections of all membranes are higher than 99.6%.

3.5. Anti-fouling property

Fig. 11 shows the fouling behavior of the M4 membrane. The membrane fluxes decrease by 50 and 60%, respectively, in a 4-h experiment as the feed solutions contain SA or SDBS pollutants. Interestingly, after the M4 membrane has been soaked in 20% H_2SO_4 for one month. The membrane fouling resistance greatly improves. This is because the unreacted amine and sulfonyl chloride groups turn into more hydrophilic amine salt or sulfonyl acid groups. The high hydrophilicity of the PSA polymer leads to better pollution resistance. Note that, the membrane fluxes can be recovered to 90% of the initial value just after washing the membrane surface with clean water.

3.6. Comparison of desalination performance among acid resistant membranes

As listed in Table 4, the M4 membrane exhibits the highest water flux, salt rejection and acid resistance among all acid resistant membranes. As compared with the PV desalination membrane where the selective layer is made by reacting BDSC with MPD and TETA [4], the water flux of the PEI/MPD/BDSC based composite membrane is five times higher without losing the NaCl rejection. This demonstrates that incorporation of PEI significantly increases membrane flux. The high desalination properties and good acid tolerance of the PSA/PSE composite membrane exhibits a great potential for acid wastewater treatment and acid concentration. Moreover, desalination property of the PEI/MPD/BDSC based PSA/PES membrane is comparable to the state of art PV desalination membranes as listed in Table 5.

4. Conclusions

In conclusion, we have prepared a series of acid resistant TFC membranes for pervaporation. The structure of the TFC membrane was optimized by adjusting the monomer composition and the IP process. Among all parameters, PEI played the most important role in the PSA layer's structure. The incorporation of PEI increased the crosslinking density and the hydrophilicity of the PSA polymer. Therefore, not only the water flux but also the ion rejection of the PSA/PES membranes increase. The best PSA/PES composite membrane with a water flux of 51.1 ± 2.3 kg m^{-2} h^{-1}, and a NaCl rejection of 99.6% was obtained. The desalination property could be maintained after soaked the membrane in 20 wt% H_2SO_4 at room temperature for one month and 20 h experiment when using a 10 wt% H_2SO_4 as feed at 75 °C. All these results proved a high potential for the PSA/PES membrane in recycling acid wastewater.

By comparing the temperature dependence of the PSA/PES membranes with 5 representative PV desalination membranes, the PSA based membrane showed the highest activation energy. This indicated that the aromatic hyper-crosslinked dense layer structure limited the water transport. Therefore, further study on improving water flux of the interfacial polymerized layer should be attempted on decreasing activation energy by increasing chain flexibility or blending 2 D materials.

Author statement

The authors declare no competing interests.

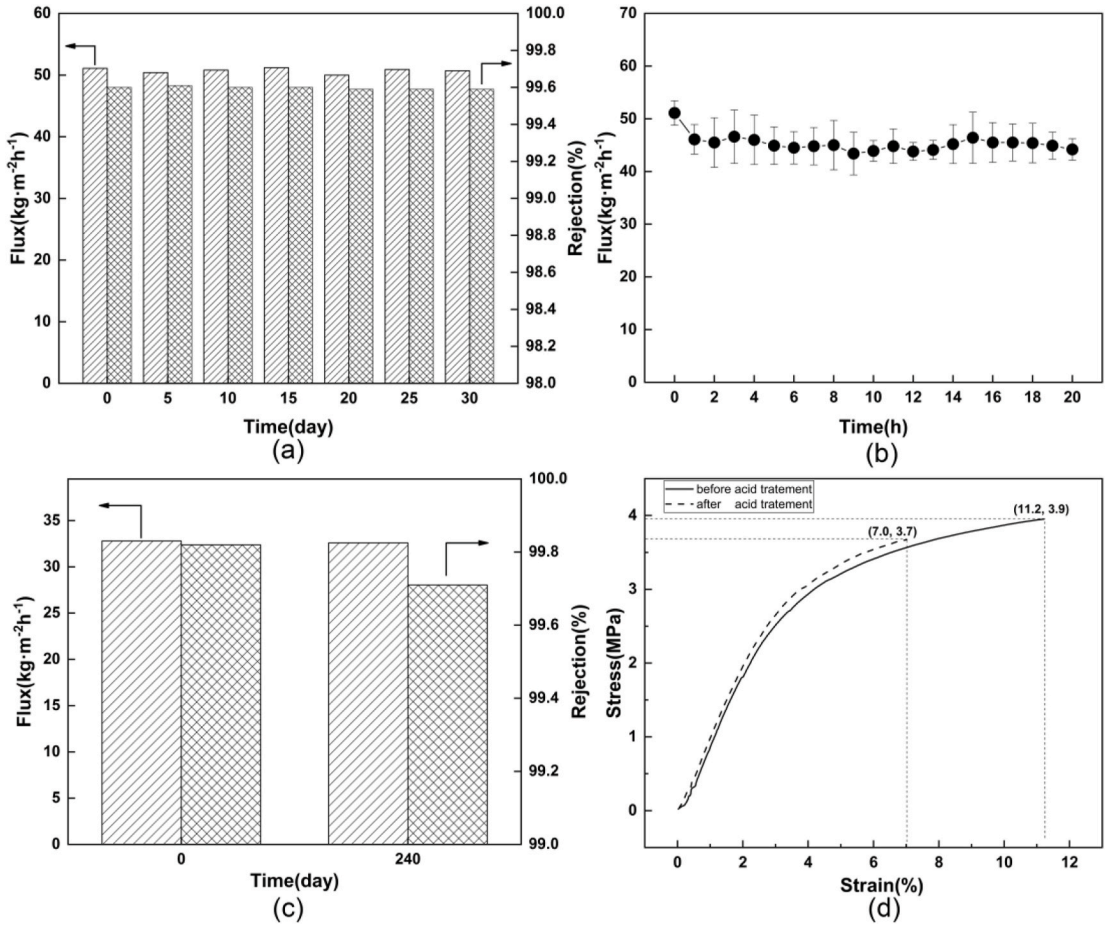

Fig. 10. The PV performances of M4 membranes underwent (a) static acid resistance 30 days and testing every 5 days, (b) dynamic acid resistance testing every 2 h, (c) M19(PE) membrane underwent 240 days static acid resistance test (the feed temperatures was 75 °C, permeate side was in a vacuum of 100 Pa). (d) stress-strain curves of membrane before and after 30 days acid treatment.

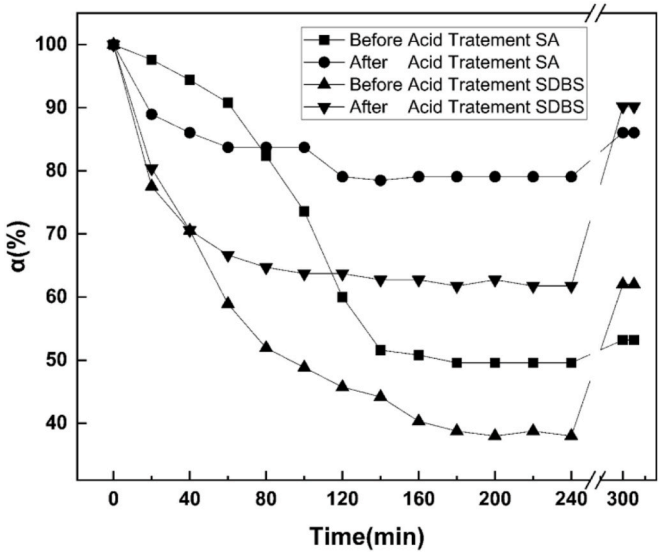

Fig. 11. The normalized flux changes over time for M4 membranes with or without being soaked in 20 wt% H_2SO_4 solution for one month. The 3.5 wt% NaCl feed solution contains 0.1 wt%, SA or SDBC. (feed temperature: 75 °C, permeate side pressure: 100 Pa).

Table 4
Desalination properties of acid resistant membranes.

Membrane type	Testing condition (wt% of H_2SO_4)	Water flux ($kg·m^{-2}·h^{-1}$)	Rejection to NaCl
PV [4]	[a] 20% and[b] 10%	10.1	99.37
NF [11]	[a] 8%	10.6	51.5–63.5%
NF [13]	[a] 20% and[b] 4.9%	5.8	50%
NF [25]	[a] 10% and[b] 5%	12.5	–
NF [30]	[a] 5%	8.68	40.5%
RO [40]	[a] 15%	14.5 ± 0.9	85.1 ± 0.9%
PV this work	[a] 20% and[b] 10%	51.1 ± 2.3	99.60 ± 0.03%

[a] Static test: the membrane was soaked in a 10 or 20 wt% H_2SO_4 solution.
[b] Dynamic test: a H_2SO_4 solution was used as the feed solution.

Table 5
The pervaporation desalination properties among representative membranes.

Membrane type	Feed temperature	Water flux ($kg·m^{-2}h^{-1}$)	Salt rejection
GO/PAN composite [36]	90 °C	65.1	99.80%
PVA/PAN composite [41]	70 °C	46.3	99.80%
UiO-66-NH_2 based membrane [42]	90 °C	12.1	99.70%
PSA/PES membrane in this work	75 °C	55.1 ± 2.3	99.60 ± 0.03%

Declaration of competing interest

The authors declare no competing financial interests.

Acknowledgement

This research is funded by National Natural Science Foundation of China (51773011).

Appendix A. Supplementary data

Supplementary data to this article can be found online at https://doi.org/10.1016/j.memsci.2021.119108.

References

[1] K. Yao, M. Jia, H. Wu, Y. Li, C. Chen, Y. Huang, Synthesis of BiOCl using Cl source from industrial wastewater and its application for wastewater treatment, Environ. Technol. 40 (2019) 374–385.
[2] S. Hong, S. Shuang, W. Haibing, Experimental study on the treatment of acid scarlet wastewater with modified bentonite, Sci. Technol. Rev. 27 (2009) 89–92.
[3] R.G. Rice, Applications of ozone for industrial wastewater treatment — a review, Ozone: Sci. Eng. 18 (1996) 477–515.
[4] K. Cui, P. Li, R. Zhang, B. Cao, Preparation of pervaporation membranes by interfacial polymerization for acid wastewater purification, Chem. Eng. Res. Des. 156 (2020) 171–179.
[5] F.W. Sousa, M.J. Sousa, I.R. Oliveira, A.G. Oliveira, R.M. Cavalcante, P.B. Fechine, V.O. Neto, D. de Keukeleire, R.F. Nascimento, Evaluation of a low-cost adsorbent for removal of toxic metal ions from wastewater of an electroplating factory, J. Environ. Manag. 90 (2009) 3340–3344.
[6] D.C. Zhang, X.L. Liu, D.M. Guan, X.Y. Xu, S.Y. Wu, Study on treatment of smelting contaminated acid by evaporation condensing process, Adv. Mater. Res. (2014) 564–569.
[7] S. Yuan, J. Li, J. Zhu, A. Volodine, J. Li, G. Zhang, P. Van Puyvelde, B. Van der Bruggen, Hydrophilic nanofiltration membranes with reduced humic acid fouling fabricated from copolymers designed by introducing carboxyl groups in the pendant benzene ring, J. Membr. Sci. 563 (2018) 655–663.
[8] N. Cao, Y. Sun, J. Wang, H. Zhang, J. Pang, Z. Jiang, Strong acid- and solvent-resistant polyether ether ketone separation membranes with adjustable pores, Chem. Eng. J. 386 (2020) 124086.
[9] S. Yu, M. Ma, J. Liu, J. Tao, M. Liu, C. Gao, Study on polyamide thin-film composite nanofiltration membrane by interfacial polymerization of polyvinylamine (PVAm) and isophthaloyl chloride (IPC), J. Membr. Sci. 379 (2011) 164–173.
[10] S. Gu, G. He, X. Wu, Y. Guo, H. Liu, L. Peng, G. Xiao, Preparation and characteristics of crosslinked sulfonated poly(phthalazinone ether sulfone ketone) with poly(vinyl alcohol) for proton exchange membrane, J. Membr. Sci. 312 (2008) 48–58.
[11] S. Yu, Q. Zhou, S. Shuai, G. Yao, M. Ma, C. Gao, Thin-film composite nanofiltration membranes with improved acid stability prepared from naphthalene-1,3,6-trisulfonylchloride (NTSC) and trimesoyl chloride (TMC), Desalination 315 (2013) 164–172.
[12] Z. Li, Z. Wang, G. Li, Preparation of nano-titanium dioxide from ilmenite using sulfuric acid-decomposition by liquid phase method, Powder Technol. 287 (2016) 256–263.
[13] M. Liu, G. Yao, Q. Cheng, M. Ma, C. Gao, Acid stable thin-film composite membrane for nanofiltration prepared from naphthalene-1,3,6-trisulfonylchloride (NTSC) and piperazine (PIP), J. Membr. Sci. 415–416 (2012) 122–131.
[14] Y. Gao, Z.H. Li, B.W. Cheng, K.M. Su, Superhydrophilic poly(p-phenylene sulfide) membrane preparation with acid/alkali solution resistance and its usage in oil/water separation, Separ. Purif. Technol. 192 (2018) 262–270.
[15] S.C. Yu, C.J Gao, Research on performance of sulfonated polyethersulfone composite nanofiltration membrane, Technol. Water Treat. 26 (2000) 63–66.
[16] C. Yan, S. Zhang, D. Yang, X. Jian, Preparation and characterization of chloromethylated/quaternized poly(phthalazinone ether sulfone ketone) for positively charged nanofiltration membranes, J. Appl. Polym. Sci. 107 (2008) 1809–1816.
[17] Y.L. Xue, C.H. Lau, C. Bing, P. Li, Elucidating the impact of polymer crosslinking and fixed carrier on enhanced water transport during desalination using pervaporation membranes, J. Membr. Sci. 575 (2019) 135–146.
[18] S.A. Ahmad, Hybrid process (pervaporation-distillation): a review, Int. J. Sci. Eng. Res. 3 (2012).
[19] D.C. Zhang, X.L. Liu, D.M. Guan, X.Y. Xu, S.Y. Wu, Study on treatment of smelting contaminated acid by evaporation condensing process, Adv. Mater. Res. 881–883 (2015) 564–569.
[20] M. Shi, Z. Wang, S. Zhao, J. Wang, S. Wang, A support surface pore structure reconstruction method to enhance the flux of TFC RO membrane, J. Membr. Sci. 541 (2017) 39–52.
[21] Y. Li, J. Xue, X. Zhang, B. Cao, P. Li, Formation of macrovoid-free PMDA-MDA polyimide membranes using a gelation/non-solvent-induced phase separation method for organic solvent nanofiltration, Ind. Eng. Chem. Res. 58 (2019) 6712–6720.
[22] Y. Li, B. Cao, P. Li, Effects of dope compositions on morphologies and separation performances of PMDA-ODA polyimide hollow fiber membranes in aqueous and organic solvent systems, Appl. Surf. Sci. 473 (2018) 1038–1048.
[23] J. Meng, P. Li, B. Cao, High-flux direct-contact pervaporation membranes for desalination, ACS Appl. Mater. Interfaces 11 (2019) 28461–28468.
[24] S.J. Davies, C.M. White, An experimental study of the flow of water in pipes of rectangular section, Proc. R. Soc. Lond. - Ser. A Contain. Pap. a Math. Phys. Character 119 (1928) 92–107.
[25] H. Hoseinpour, M. Peyravi, A. Nozad, M. Jahanshahi, Static and dynamic assessments of polysulfonamide and poly(amide-sulfonamide) acid-stable membranes, Journal of the Taiwan Institute of Chemical Engineers (2016) 453–466.
[26] J.A. Dean, Analytical Chemistry Handbook, 1995.
[27] M. Cho, S.H. Lee, D. Lee, D.P. Chen, I. Kim, M.S. Diallo, Osmotically driven membrane processes: exploring the potential of branched polyethyleneimine as draw solute using porous FO membranes with NF separation layers, J. Membr. Sci. 511 (2016) 278–288.
[28] G.A. Schick, Z. Sun, Spectroscopic characterization of sulfonyl chloride immobilization on silica, Langmuir 10 (1994) 3105–3110.
[29] K. Wang, Y. Qin, S. Quan, Y. Zhang, P. Wang, H. Liang, J. Ma, X.Q. Cheng, Development of highly permeable polyelectrolytes (PEs)/UiO-66 nanofiltration membranes for dye removal, Chem. Eng. Res. Des. 147 (2019) 222–231.
[30] Y. Zeng, L. Wang, L. Zhang, J. Yu, An acid resistant nanofiltration membrane prepared from a precursor of poly(s-triazine-amine) by interfacial polymerization, J. Membr. Sci. 546 (2018) 225–233.
[31] R.J. Good, A thermodynamic derivation of wenzel's modification of young's equation for contact angles; together with a theory of Hysteresis1, J. Am. Chem. Soc. 74 (1952) 5041–5042.
[32] J.Y. Lee, S.O. Hwang, H.-J. Kim, D.-Y. Hong, J.S. Lee, J.-H. Lee, Hydrosilylation-based UV-curable polydimethylsiloxane pervaporation membranes for n-butanol recovery, Separ. Purif. Technol. 209 (2019) 383–391.
[33] Y.L. Xue, J. Huang, C.H. Lau, B. Cao, P. Li, Tailoring the molecular structure of crosslinked polymers for pervaporation desalination, Nat. Commun. 11 (2020) 1–9.
[34] Q. Li, B. Cao, P. Li, Fabrication of high performance pervaporation desalination composite membranes by optimizing the support layer structures, Ind. Eng. Chem. Res. 57 (2018) 11178–11185.
[35] J. Meng, C.H. Lau, Y. Xue, R. Zhang, B. Cao, P. Li, Compatibilizing hydrophilic and hydrophobic polymers via spray coating for desalination, J. Mater. Chem. 8 (2020) 8462–8468.
[36] B. Liang, W. Zhan, G. Qi, S. Lin, Q. Nan, Y. Liu, B. Cao, K. Pan, High performance graphene oxide/polyacrylonitrile composite pervaporation membranes for desalination applications, J. Mater. Chem. 3 (2015) 5140–5147.
[37] G. Liu, J. Shen, Q. Liu, G. Liu, J. Xiong, J. Yang, W. Jin, Ultrathin two-dimensional MXene membrane for pervaporation desalination, J. Membr. Sci. 548 (2018) 548–558.
[38] Y. Song, P. Sun, L.L. Henry, B. Sun, Mechanisms of structure and performance controlled thin film composite membrane formation via interfacial polymerization process, J. Membr. Sci. 251 (2005) 67–79.
[39] A. Droudian, S.K. Youn, L.A. Wehner, R.M. Wyss, M. Li, H.G. Park, Enhanced chemical separation by freestanding CNT–polyamide/imide nanofilm synthesized at the vapor–liquid interface, ACS Appl. Mater. Interfaces 10 (2018) 19305–19310.
[40] M.G. Shin, S.J. Kwon, H. Park, Y.-I. Park, J.-H. Lee, High-performance and acid-resistant nanofiltration membranes prepared by solvent activation on polyamide reverse osmosis membranes, J. Membr. Sci. 595 (2020) 117590.
[41] B. Liang, Q. Li, B. Cao, P. Li, Water permeance, permeability and desalination properties of the sulfonic acid functionalized composite pervaporation membranes, Desalination 433 (2018) 132–140.
[42] L. Wan, C. Zhou, K. Xu, B. Feng, A. Huang, Synthesis of highly stable UiO-66-NH2 membranes with high ions rejection for seawater desalination, Microporous Mesoporous Mater. 252 (2017) 207–213.